IEEE Access
Multidisciplinary | Rapid Review | Open Access Journal

Received December 26, 2020, accepted January 2, 2021, date of publication January 5, 2021, date of current version January 19, 2021.

*Digital Object Identifier 10.1109/ACCESS.2021.3049374*

# Study of AlGaN/GaN Vertical Superjunction HEMT for Improvement of Breakdown Voltage and Specific On-Resistance

**MIAO ZHANG[1], ZHIYOU GUO[1], YONG HUANG[2], YUAN LI[1], JIANCHENG MA[1], XIAOYU XIA[1], XIUYANG TAN[1], FAN XIA[1], AND HUIQING SUN[1]**

[1]Institute of Semiconductor Science and Technology, South China Normal University, Guangzhou 510631, China
[2]Guangdong Polytechnic Normal University, Guangzhou 510665, China

Corresponding author: Zhiyou Guo (guozy@scnu.edu.cn)

This work was supported in part by the Key-Area Research and Development Program of Guangdong Province under Grant 2019B010128002 and Grant 2020B010171002, in part by the Foshan Science and Technology Bureau under Grant 1920001000724, in part by the Guangdong Science and Technology Project under Grant 2019KTSCX084, and in part by the Guangzhou Science and Technology Program Key Projects under Grant 201807010083.

**ABSTRACT** A GaN-based vertical superjunction high electron mobility transistor (SJ HEMT) with a composite structure (CS-SJ HEMT) is proposed and analyzed by Silvaco TCAD to improve the breakdown voltage and specific on-resistance ($R_{onA}$). In this paper, CS-SJ HEMT is compared with SJ HEMT with traditional structure (TS-SJ HEMT), SJ HEMT with only particular doping pillars (DP-SJ HEMT) and SJ HEMT with only special P-gate (SP-SJ HEMT). The particular doping pillars mean the doping concentration of n-pillar increases with a gradient from top to bottom, and the concentration of p-pillar is the same as the middle of n-pillar, which reduces the $R_{onA}$ by only 4%. The special P-GaN cap layer can reduce the $R_{onA}$ by 10%, and it can even increase the on-state current in the saturation region. The CS-SJ HEMT combines both doping pillars and special P-gate structures, and the $R_{onA}$ can be reduced by 14%. By the optimized design, the $R_{onA}$ can be reduced by 30% with BV = 2580 V, or the $R_{onA}$ can be reduced by 21% with BV = 2720 V. These results show that the composite structure of SJ HEMT contributes to improving the BV and $R_{onA}$ and propose a useful approach for improving the vertical HEMTs.

**INDEX TERMS** GaN-based vertical SJ HEMT, particular doping pillars, special P-gate, specific on-resistance, breakdown voltage.

## I. INTRODUCTION

As a representative of the III-nitride material, GaN has a wide band, high electron saturation drift velocity, high electron mobility, high critical field strength, high thermal conductivity and other excellent physical properties, so it has become an ideal power electronic material [1]–[5]. Compared with traditional Si materials, power-switching devices based on GaN power electronic materials have higher power density output and energy conversion efficiency. They can make the system smaller and lighter, effectively reducing the size and weight of power electronic devices [6]–[9], thus greatly reducing system fabrication and production costs. It has a huge market application prospect.

In recent years, vertical GaN-based HEMT devices [10]–[12] have attracted much attention in the field of high-power electronics with their excellent performance. Research on what methods are used to improve the conduction characteristics of vertical devices has become a hot spot in this field. The introduction of structures such as P-buried layer [13], superjunction (SJ) [14]–[17] and current barrier layer (CBL) of $SiO_2$ material [18] has promoted the improvement of vertical device performance and laid the foundation for the current demand for a wider range of applications. However, the existing technology to reduce the specific on-resistance ($R_{onA}$) of vertical devices is still relatively limited. Therefore, how to solve the above problems better and improve the performance of power devices further is the focus of attention of many scholars in the world, and it is also the research focus of this paper.

The associate editor coordinating the review of this manuscript and approving it for publication was Gian Domenico Licciardo.

In this paper, a GaN-based vertical superjunction high electron mobility transistor (SJ HEMT) with a composite structure (CS-SJ HEMT) is proposed and analyzed. In order to study this structure, SJ HEMT with traditional structure (TS-SJ HEMT) is compared to SJ HEMT with only particular doping pillars (DP-SJ HEMT), SJ HEMT with only special P-gate (SP-SJ HEMT) and CS-SJ HEMT. Compared with traditional structure, the doping concentration differences between p/n-pillar can reduce the $R_{onA}$ while the special P-gate can reduce the $R_{onA}$ and increase the on-state current in the saturation region. Then TS-SJ HEMT is compared with CS-SJ HEMT to confirm whether the composite structure impacts breakdown voltage (BV). Two-dimensional device simulation using Silvaco-TCAD software reveals its intrinsic operation mechanism by exploiting the potential distribution, electric field distribution and current density distribution. These results have important implications for the optimization and design of GaN-based vertical HEMTs.

## II. DEVICE STRUCTURES AND PARAMETERS

According to Ref. [14], Z. Li and T. P. Chow have designed and analyzed an original kind of GaN vertical superjunction HEMT, so the model and some parameters can refer to it. The device structures proposed in this paper have been calibrated by previous experimental results [19].

Fig. 1 shows four kinds of the half-cell schematic cross-section of the proposed structure. There is only one difference between each of the two device structures for comparison, and their important parameters are given in Table 1. The GaN epi layer is divided into left and right parts from the middle, with an Mg-doped p-pillar on the left and several Si-doped n-pillars on the right. In TS-SJ HEMT, all the p/n-pillar is a uniform doping concentration of $N_1$, and it is the same as SP-SJ HEMT. As for the other two device structures, both n-pillars have a consistent doping gradient, namely $N_1$, $N_2$, $N_3$, $N_4$, and $N_5$, determined from top to bottom in each gradient layer, while the concentration of p-pillar is the same as the middle of n-pillar. The sum of the thickness of all small n-pillars is 10 $\mu$m, and the thickness of each small n-pillar can be the same. The Al composition in the $Al_xGa_{1-x}N$ barrier layer is closely related to the polarization charge. When x is too high, the large lattice and thermal mismatch between the GaN buffer layer and the barrier layer cause the high structural defect density and rough interface in AlGaN to limit the mobility of 2DEG; when x is too low, the difference of conduction band energy will become very small, resulting in no good limit on the carrier concentration. $Al_{0.1}Ga_{0.9}N$ may be chosen as the barrier layer after analyzing the results in Refs. [20] and [21]. This is because the 2DEG must be fully depleted under 0V gate bias by the P-GaN cap to reduce the electric field under the gate in off-state and achieve an enhancement operation mode of the device [14]. The special P-gate is only in SP-SJ HEMT and CS-SJ HEMT for comparison. The gate looks like the letter 'T', and the Mg-doped [22]–[24] p-type GaN cap layer is divided into two pieces with the same size $T_c$. The bottom of the gate and the top of the AlGaN barrier layer are separated by SiN. Except for the above differences, other device structures are the same in both doping concentration and shape.

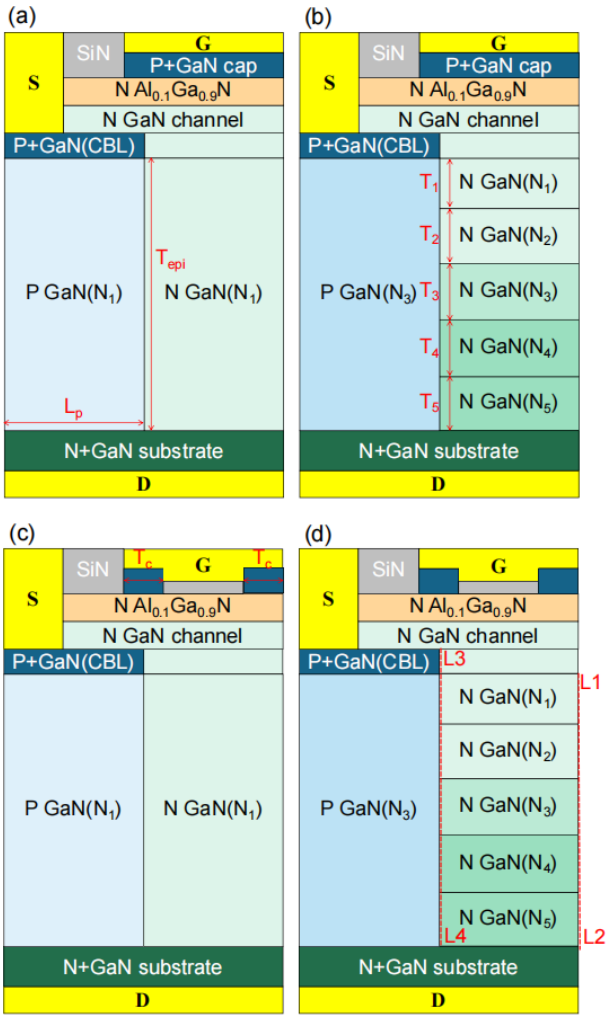


**FIGURE 1.** Device structure (a) TS-SJ HEMT (b) DP-SJ HEMT (c) SP-SJ HEMT (d) CS-SJ HEMT. ($T_n = T_{epi}/5$) Lines L1L2 or L3L4 represent the vertical direction of n-pillar junction or the middle of the structure, respectively.

Silvaco-TCAD software is considered a tool for two-dimensional numerical simulations. The concentration-dependent recombination model is used for concentration-dependent lifetimes. At high current densities, it is important to use the Auger recombination model for the direct transition of three carriers. In order to simulate the generation of 2DEG, the polarization effect [25], [26] must be considered at the interface of the $Al_{0.1}Ga_{0.9}N$ barrier layer and GaN channel layer. The effect also applies to the P-GaN cap layer and $Al_{0.1}Ga_{0.9}N$ barrier layer to deplete 2DEG under the cap layer. The Faramand Modified Caughey Thomas model and Nitride Field Dependent model are also used for electrons and holes [27], [28]. Besides, Selberherr' s Impact Ionization model is used for calculating breakdown voltage.

**TABLE 1. Key parameters for the simulations.**

| Symbol | Quantity | Value |
|---|---|---|
| $T_{cap}$ | P-GaN cap thickness | 200 nm |
| $N_{cap}$ | P-GaN cap doping concentration (Mg-doped) | $1\times10^{18}$ cm$^{-3}$ |
| $T_{AlGaN}$ | $Al_{0.1}Ga_{0.9}N$ thickness | 25 nm |
| $T_{channel}$ | GaN channel thickness | 100 nm |
| $T_{CBL}$ | CBL thickness | 1 μm |
| $N_{CBL}$ | CBL doping concentration (Mg-doped) | $1\times10^{18}$ cm$^{-3}$ |
| $T_{epi}$ | Epi-layer thickness | 10 μm |
| $L_p$ | Length of the p-pillar | 8 μm |
| $T_n$ | Thickness of each doping gradient | 0∼10 μm ($\sum_{n=1}^{5} T_n = T_{epi}$) |
| $T_c$ | Length of the special cap layer | 0.1∼6 μm |
| $N_1$ | Initial doping concentration of p/n-pillar (Mg/Si-doped) | $0.5\times10^{16}\sim1.5\times10^{16}$ cm$^{-3}$ |
| $N_{step}$ | Doping concentration increment of n-pillar | $0\sim2\times10^{16}$ cm$^{-3}$ |
| $N_n$ | Doping concentration after increasing (Si-doped) | $N_1+(n-1)\times N_{step}$ |

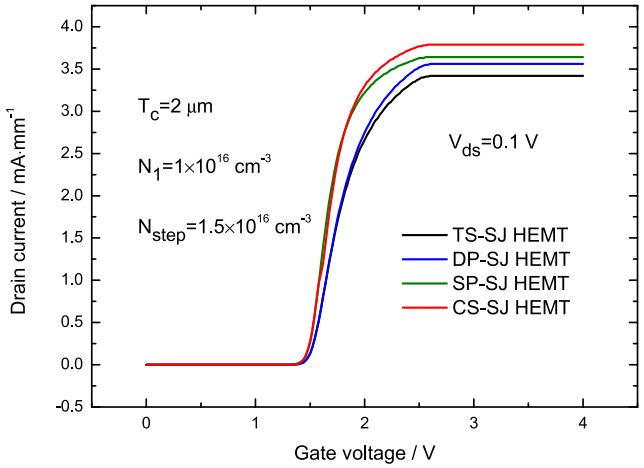


**FIGURE 2. On-State transfer I-V characteristics for four devices.**

## III. ON-STATE AND OFF-STATE ANALYSES

The on-state I-V characteristics for TS-SJ HEMT, DP-SJ HEMT, SP-SJ HEMT and CS-SJ HEMT are shown in Fig. 2 and 3. According to Fig. 2, these devices have the same threshold voltage of 1.4 V, so neither special P-gate nor doping pillars have an effect on the threshold voltage. When the gate voltage is beyond the threshold voltage, the drain current of TS-SJ HEMT is the lowest among the four devices, which means it has the largest on-state resistance. The drain current of two structures with special P-gates is much higher than that of the other two devices, while the drain current of two structures with the doping pillars is a bit higher than that of the other two devices. In other words, the CS-SJ HEMT has the smallest on-state resistance among these structures. In Fig. 3(a), the I-V curve shows that the slope of the traditional structure is smaller than that of another structure. The $R_{onA}$ of the traditional structure is 4.01 mΩ·cm$^2$, while the $R_{onA}$ of DP-SJ HEMT is 3.86 mΩ·cm$^2$, which means the latter is 4% lower than the former. The $R_{onA}$ of SP-SJ

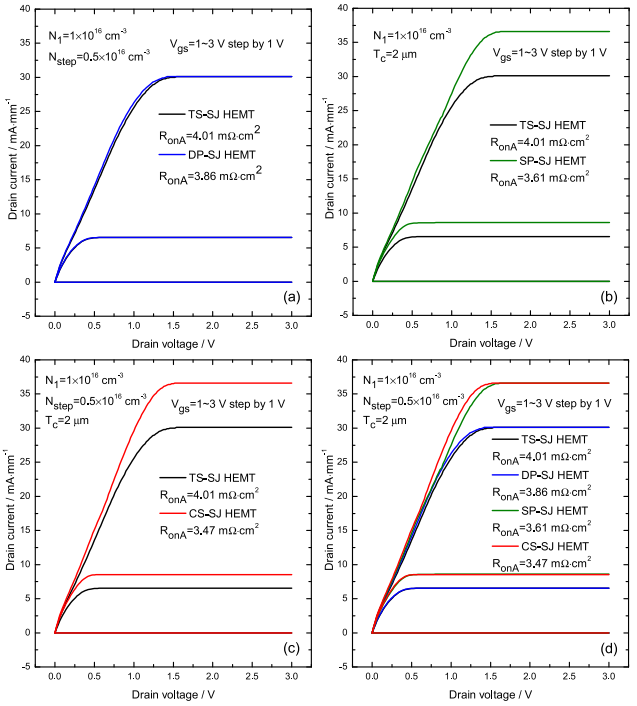


**FIGURE 3. On-State output I-V characteristics. TS-SJ HEMT is compared with (a) DP-SJ HEMT, (b) SP-SJ HEMT, and (c) CS-SJ HEMT, as well as (d) comparison at the same time.**

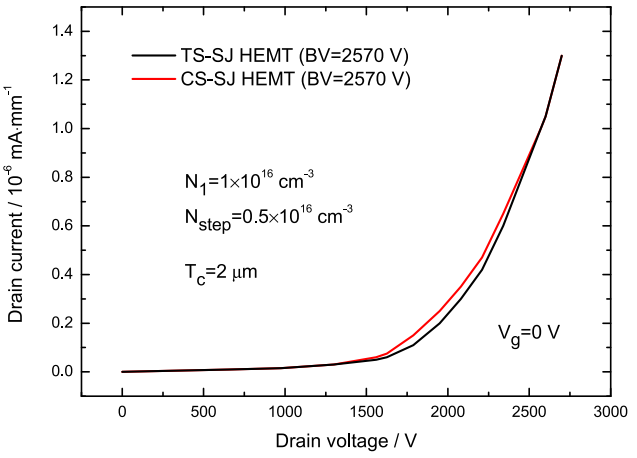


**FIGURE 4. Off-State I-V characteristics. CS-SJ HEMT is compared with TS-SJ HEMT.**

HEMT is 3.61 mΩ·cm$^2$, and it is 10% lower than that of the traditional structure in Fig. 3(b). Similarly, the $R_{onA}$ of CS-SJ HEMT is 3.47 mΩ·cm$^2$, and it is 14% lower than that of the traditional structure in Fig. 3(c). They are all shown in Fig. 3. Besides, in the saturation region, the on-state current of the structures with special P-gates is higher than that of the structures without P-gates. In Fig. 4, when $V_g = 0$ V, the off-state I-V curves look similar. If the current of the device is higher than $1 \times 10^{-6}$ mA·mm$^{-1}$ on the off-state, it is considered to be broken down. Fig. 4 performs that both structures have the same BV = 2570 V, which proves the composite structure can reduce $R_{onA}$ while having few influences on BV.

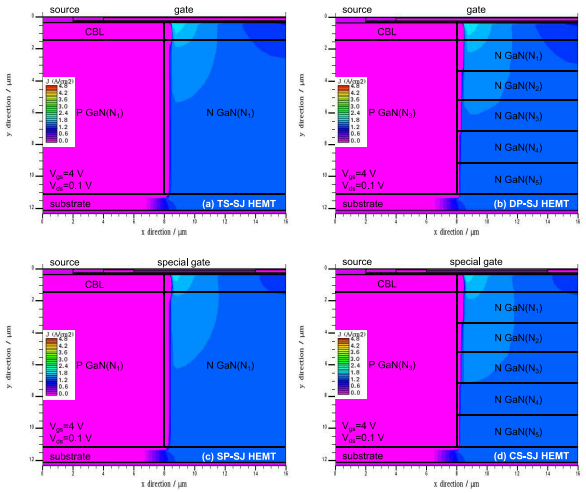


**FIGURE 5.** On-State current density two-dimensional distributions for (a) TS-SJ HEMT, (b) DP-SJ HEMT, (c) SP-SJ HEMT and (d) CS-SJ HEMT. The value of the current density is in the log scale.

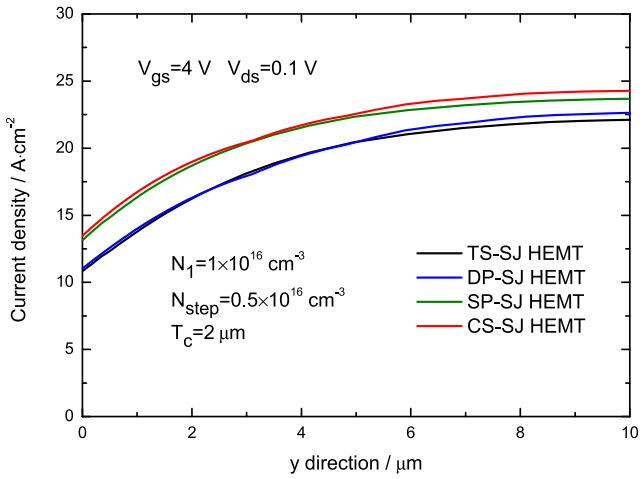


**FIGURE 6.** On-State current density along epi layer (line L1L2) as shown in Fig. 1 for four devices.

Though physical observation, the status of the device could be clearly understood according to current density, electric field and equipotential surface. In Fig. 5, the current density only exists in the right half of the device during on-state, which means the current path is along the n-pillar instead of the p-pillar. The current cannot flow into the p-pillar because the PN junctions formed by p-pillar/n-pillar and p-pillar/N-GaN substrate are both under reverse bias conditions. The current along the top of the n-pillar is cut down from left to right by the depletion effect [29], [30]. The special P-gate can shrink the depletion region on the right significantly, so the current density can be increased using this method. The boundary between the p-pillar and n-pillar of the device with doping pillars is different from the device without pillars, proving it could improve current density through widening effective current path [30]. As shown in Fig. 6, the device with composite structure has the highest current density in the epi layer, which means both structures are

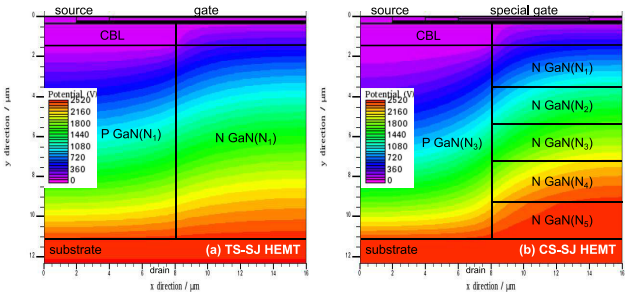


**FIGURE 7.** Off-State performance of (a) TS-SJ HEMT compared with (b) CS-SJ HEMT according to equipotential surface.

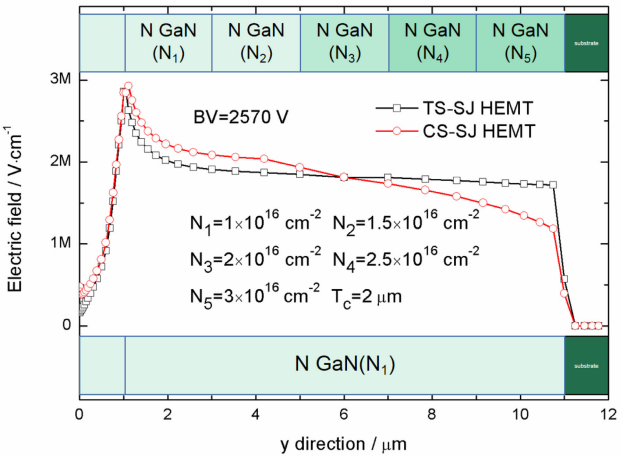


**FIGURE 8.** Off-State performance of TS-SJ HEMT compared with CS-SJ HEMT according to electric field distribution along line L3L4 as shown in Fig. 1.

good for current transmission with the reduction of $R_{onA}$. The breakdown state of TS-SJ HEMT and CS-SJ HEMT is illustrated in Fig. 7 and Fig. 8. The equipotential surfaces of both structures are shown in Fig. 7. The high equipotential-area of the former near the bottom of n-pillar is higher than that of the latter. It means that the electric field strength of the upper pillar is enhanced while that of the lower pillar is weakened, which could be demonstrated by the vertical electric field distributions along the line L1L2 in Fig. 8. The area beneath the contour of each electric field distribution can be used to estimate the BV of each device approximately [14], [31]. As Fig. 8 shown, the value of the electric field of CS-SJ HEMT is greater than TS-SJ HEMT in the upper part of the pillar, while smaller in the lower part of the pillar. Equal areas can be found as shown, so it represents the same BV = 2570 V.

## IV. OPTIMIZATION AND DISCUSSION FOR MINIMIZED SPECIFIC ON-RESISTANCE

Fig. 9 shows the relationship of the optimized BV and $R_{onA}$ versus length $T_c$ for given $N_1$ and $N_{step}$ in structures. It is worth noting that the structure will be considered as TS-SJ HEMT or DP-SJ HEMT when $T_c = 6\mu$m. As shown, the $R_{onA}$ of the device with particular doping pillars is lower than that of the device without pillars, but BV is almost the same, which means this doping method has little impact on

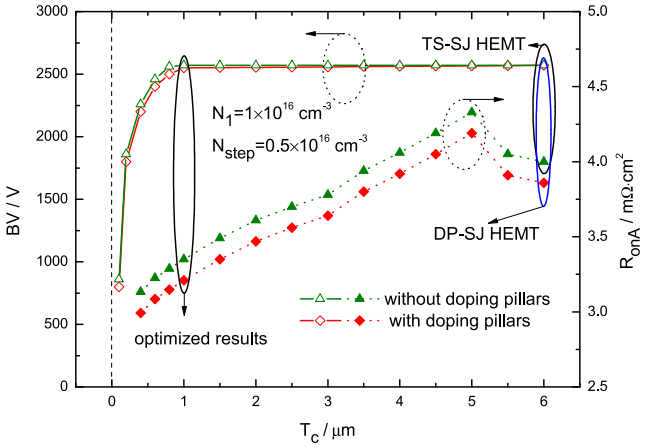


**FIGURE 9.** Relationship of the optimized BV and $R_{onA}$ versus length $T_c$ in different devices.

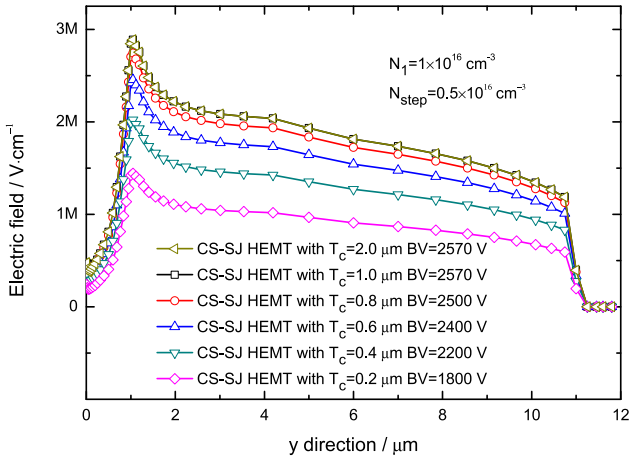


**FIGURE 10.** Electric field distributions along the line L3L4 corresponding to CS-SJ HEMT at the breakdown voltage with different values of $T_c$ in Fig. 8.

BV with $N_1 = 1 \times 10^{16}$ cm$^{-3}$ and $N_{step} = 0.5 \times 10^{16}$ cm$^{-3}$. There is a peak $R_{onA}$ with $T_c = 5\mu$m whether having particular doping pillars or not, and $R_{onA}$ decreases monotonically with the decreasing $T_c$. BV is almost unchanged before $T_c$ decreases to 1 $\mu$m, and when $T_c$ is less than 1 $\mu$m, BV drops off a cliff. The optimized $T_c$ depends on minimizing $R_{onA}$ with less reduction of BV, and it is easy to find that the optimized $T_c$ seems to be close to 1 $\mu$m. For a given $N_1$ and $N_{step}$, the BV of the structure will remain the same if $T_c$ is higher than the optimal value, while the BV will decrease a lot if $T_c$ is lower than the optimal value. These changes of the breakdown voltage in different structures can be illustrated in Fig. 10. As shown, although the values of $T_c$ are different, the shapes of the electric field distributions are almost the same. When $T_c$ is more than 1 $\mu$m, there is no further change in the curve, and the potential of the device with $T_c = 2\mu$m is as same as the traditional device in Fig. 11, which means BV remains unchanged. Because the distance between the gate and drain does not change, and the thickness of the epi layer has no change. Besides, the length of the exhausted 2DEG is long enough to keep the off-state. As $T_c$ decreases to less

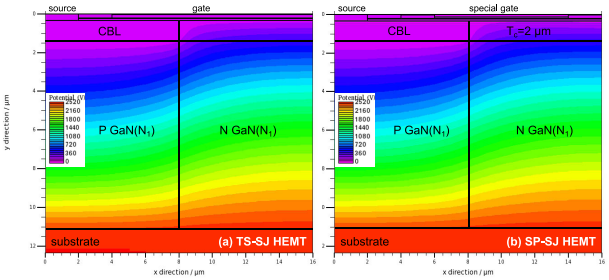


**FIGURE 11.** Off-State performance of (a) TS-SJ HEMT compared with (b) SP-SJ HEMT($T_c = 2\mu$m) according to equipotential surface.

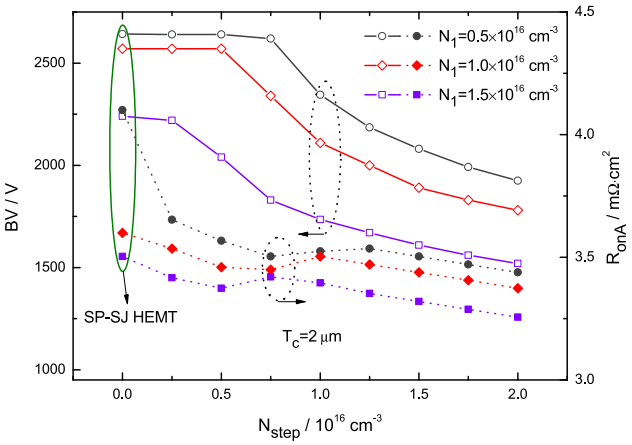


**FIGURE 12.** Relationship of the optimized BV and $R_{onA}$ versus the $N_{step}$ in different devices.

than 1 $\mu$m, the electric field strength also drops to a certain degree because the device is easily broken down if the length of the exhausted 2DEG under the gate is too short. Therefore, it is very important to choose a suitable value of $T_c$ to balance the lower $R_{onA}$ and higher BV.

Fig. 12 shows the relationship of the optimized BV and $R_{onA}$ versus the $N_{step}$ for given $T_c$. The structure could be considered as SP-SJ HEMT when $N_{step} = 0$. As shown in the figure, both BV and $R_{onA}$ will decrease with the increasing $N_1$, consistent with the reported results [29], [30]. When the $N_{step}$ is low enough, the BV of the structure remains unchanged. However, as $N_1$ gradually increases, the critical value of $N_{step}$ for keeping BV unchanged will decrease by degrees. It should be noted that the $R_{onA}$ of the structure has a rebound zone, which means the $R_{onA}$ is not always in a downward trend with the increasing $N_{step}$.

The relationship of the optimized BV and $R_{onA}$ versus length $T_3$ for given $N_1$ and $N_{step}$ is shown in Fig. 13. According to Ref. [29] and previous experimental results, the average concentration of the n-pillar will directly affect BV and $R_{onA}$, so it is important to keep the thickness of the gradient concentration on the upper and lower sides symmetrically the same ($T_1 = T_2 = T_3 = T_4$). As shown, BV is improved if $T_3$ is greater than 2 $\mu$m and less than 8 $\mu$m, and there is a peak BV with $T_3 = 3\mu$m. When $T_3$ is between 2 $\mu$m and 5 $\mu$m, the $R_{onA}$ remains unchanged for the time being. In other cases, $R_{onA}$ decreases as $T_3$ increases. Therefore,

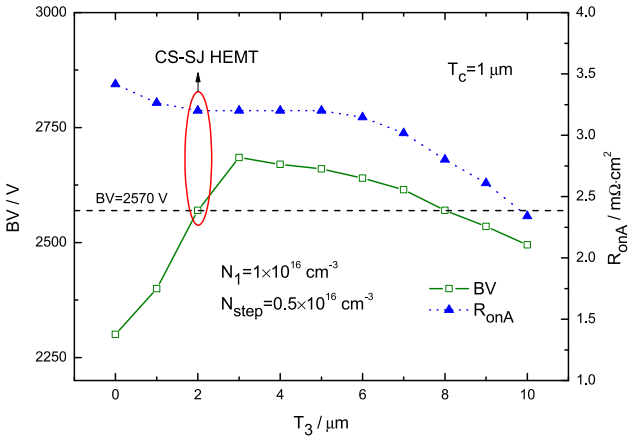


**FIGURE 13.** Relationship of the optimized BV and $R_{onA}$ versus the $T_3$ in CS-SJ HEMT.($T_1 = T_2 = T_3 = T_4$).

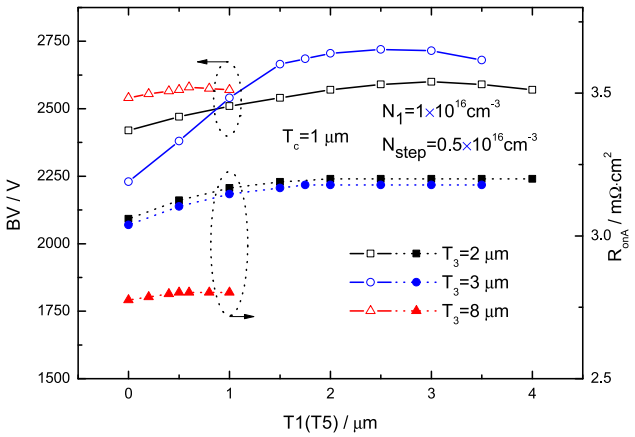


**FIGURE 14.** Relationship of the optimized BV and $R_{onA}$ versus the $T_1(T_5)$ in CS-SJ HEMT.($T_1 = T_5, T_2 = T_4$).

the optimal value of $T_3$ should be 3 $\mu$m or 8 $\mu$m according to the requirements of BV and $R_{onA}$. Fig. 14 is a further optimization based on several optimized values in Fig. 13. When $T_3 = 3\mu$m and $T_1(T_5) = 2.5\mu$m, the BV can increase to 2720 V, and $R_{onA}$ can decrease to 3.18 mΩ·cm$^2$, which means it is reduced by 21%; when $T_3 = 8\mu$m and $T_1(T_5) = 0.6\mu$m, the BV can increase to 2580 V, and $R_{onA}$ can decrease to 2.80 mΩ·cm$^2$, which means it is reduced by 30%.

From the above results, the BV and $R_{onA}$ can be improved further for these structures. The $R_{onA}$ could be decreased easily by reducing the length of the P-GaN cap layer or using different doping concentration and thickness of the pillars, while the BV need to remain unchanged by choosing the value of $T_c$ not less than 1 $\mu$m, appropriate $N_{step}$ and thickness of small pillars. The particular doping pillars and the special P-gate will not have a negative effect on each other, so the composite structure is feasible.

## V. FABRICATION PROCESS

At present, devices with thick GaN layers can be fabricated by GaN growth technology [32]. However, the most difficult thing is to grow p-pillars and n-pillars of the superjunctions because both p-pillars and n-pillars need to be grown alternately. GaN-based selective area growth technologies (SAG) [33], [34] is a viable way to realize the growth, which means one pillar is grown and another pillar is masked. SAG has been considered as a general method to fabricate devices with superjunctions.

According to the method mentioned in the Refs. [35] and [36], the method of GaN secondary growth to fabricate the proposed CS-SJ HEMT is given below. First, metal organic chemical vapor deposition (MOCVD) was used to deposit an Mg-doped [37], [38] p-type GaN pillar with a thickness of $T_{epi}$ and a concentration of $N_3$ on an n-type GaN substrate, which allows the fabrication of vertical p-n junctions with low-doped high-mobility drift layers. A trench with a length of $2L_p$ and a thickness of $T_{epi}$ is formed in the middle by the chlorine-based inductively coupled plasma (ICP) dry etching recipe with a very low RF power, and the UV-chemical treatment was used to treat it before the regrowth process [36]. Second, the p-type GaN pillar is masked, and several small Si-doped n-type GaN pillars with a thickness of $T_n$ and a concentration of $N_n$ are regrown by SAG to finish the p-n junctions. After UV-chemical treatment, a CBL layer with a thickness of $T_{CBL}$ and a concentration of $N_{CBL}$ is grown on the p-type GaN pillar by MOCVD, and it is etched by ICP etching to form a second trench. Then CBL layer is masked, and an n-type GaN layer with a concentration of $N_1$ is regrown to fill the trench. Third, n-type GaN channel layer, n-type $Al_{0.1}Ga_{0.9}N$ barrier layer, and p-type GaN cap layer are grown respectively by MOCVD after the source region is masked. Several trenches are formed by etching the cap layer, and the passivation layer is deposited by plasma-enhanced chemical vapor deposition (PECVD). Then, the passivation layer on and between the cap layers need to be etched. Finally, the source, drain, and gate contact metal are deposited to finish the device.

## VI. CONCLUSION

In this paper, a GaN-based vertical superjunction high electron mobility transistor with a composite structure is proposed and analyzed by Silvaco TCAD to improve the BV and $R_{onA}$. The on-state and off-state performance of the device and the physical mechanism are systematically studied and analyzed to make an optimization design. The simulation results show that the improvement of $R_{onA}$ and BV could be realized by modulating the length of the P-GaN cap layer, the doping concentration of gradient and thickness of n-pillars in CS-SJ HEMT. These results implicate the potential and advantage of CS-SJ HEMT in high power gallium nitride device.

## REFERENCES

[1] T. P. Chow and R. Tyagi, "Wide bandgap compound semiconductors for superior high-voltage unipolar power devices," *IEEE Trans. Electron Devices*, vol. 41, no. 8, pp. 1481–1483, Aug. 1994.

[2] Y. Hao, L. Yang, X. Ma, J. Ma, M. Cao, C. Pan, C. Wang, and J. Zhang, "High-performance microwave gate-recessed AlGaN/AlN/GaN MOS-HEMT with 73% power-added efficiency," *IEEE Electron Device Lett.*, vol. 32, no. 5, pp. 626–628, May 2011.

[3] M. Ishida, T. Ueda, T. Tanaka, and D. Ueda, "GaN on Si technologies for power switching devices," *IEEE Trans. Electron Devices*, vol. 60, no. 10, pp. 3053–3059, Oct. 2013.

[4] D. S. Lee, Z. Liu, and T. Palacios, "GaN high electron mobility transistors for sub-millimeter wave applications," *Jpn. J. Appl. Phys.*, vol. 53, no. 10, Oct. 2014, Art. no. 100212.

[5] U. K. Mishra, P. Parikh, and Y.-F. Wu, "AlGaN/GaN HEMTs—An overview of device operation and applications," *Proc. IEEE*, vol. 90, no. 6, pp. 1022–1031, Jun. 2002.

[6] N. Tipirneni, A. Koudymov, V. Adivarahan, J. Yang, G. Simin, and M. A. Khan, "The 1.6-kV AlGaN/GaN HFETs," *IEEE Electron Device Lett.*, vol. 27, no. 9, pp. 716–718, Sep. 2006.

[7] R. Vetury, N. Q. Zhang, S. Keller, and U. K. Mishra, "The impact of surface states on the DC and RF characteristics of AlGaN/GaN HFETs," *IEEE Trans. Electron Devices*, vol. 48, no. 3, pp. 560–566, Mar. 2001.

[8] A. M. Wells, M. J. Uren, R. S. Balmer, K. P. Hilton, T. Martin, and M. Missous, "Direct demonstration of the 'virtual gate' mechanism for current collapse in AlGaN/GaN HFETs," *Solid-State Electron.*, vol. 49, no. 2, pp. 279–282, Feb. 2005.

[9] F. Zhang, Y. Wang, X. Wu, and F. Cao, "An SEB hardened AlGaN/GaN HEMT with barrier interlayer," *IEEE Access*, vol. 8, pp. 12445–12451, Jan. 2020.

[10] N. M. Shrestha, Y. Li, and E. Y. Chang, "Optimal design of the multiple-apertures-GaN-based vertical HEMTs with $SiO_2$ current blocking layer," *J. Comput. Electron.*, vol. 15, no. 1, pp. 154–162, Mar. 2016.

[11] S. Chowdhury, M. H. Wong, B. L. Swenson, and U. K. Mishra, "CAVET on bulk GaN substrates achieved with MBE-regrown AlGaN/GaN layers to suppress dispersion," *IEEE Electron Device Lett.*, vol. 33, no. 1, pp. 41–43, Jan. 2012.

[12] Y. Zhang, M. Sun, Z. Liu, D. Piedra, H.-S. Lee, F. Gao, T. Fujishima, and T. Palacios, "Electrothermal simulation and thermal performance study of GaN vertical and lateral power transistors," *IEEE Trans. Electron Devices*, vol. 60, no. 7, pp. 2224–2230, Jul. 2013.

[13] M. Sugimoto, H. Ueda, M. Kanechika, N. Soejima, T. Uesugi, and T. Kachi, "Vertical device operation of AlGaN/GaN HEMTs on free-standing n-GaN substrates," in *Proc. Power Convers. Conf.*, Nagoya, Japan, Jun. 2007, pp. 368–372.

[14] Z. Li and T. P. Chow, "Design and simulation of 5–20-kV GaN enhancement-mode vertical superjunction HEMT," *IEEE Trans. Electron Devices*, vol. 60, no. 10, pp. 3230–3237, Oct. 2013.

[15] Z. Li and T. P. Chow, "Robustness of GaN vertical superjunction HEMT," in *Proc. 25th Int. Symp. Power Semiconductor Devices IC's (ISPSD)*, May 2013, pp. 217–220.

[16] P. Nautiyal, A. Agrawal, S. Kumari, H. Sahu, A. Naugarhiya, and S. Verma, "Electrical characteristic investigation of variation vertical doping superjunction UMOS," in *Proc. IEEE 16th India Council Int. Conf. (INDICON)*, Dec. 2019, pp. 1–4.

[17] X. Zhou and T. P. Chow, "Performance limits of 2H-GaN vertical superjunction Schottky rectifiers, MOSFETs and HEMTs," in *Proc. Compound Semiconductor Week*, Aug. 2019, pp. 1–2.

[18] N. Zeng, Y. Yin, K. Li, F. Liao, and H. Huang, "Polarization doping modulated heterojunction electron gas in AlGaN/GaN CAVETs," *Semicond. Sci. Technol.*, vol. 35, no. 9, Sep. 2020, Art. no. 095032.

[19] W. Saito, I. Omura, S. Aida, S. Koduki, M. Izumisawa, H. Yoshioka, and T. Ogura, "High breakdown voltage (>1000 V) semi-superjunction MOSFETs using 600-V class superjunction MOSFET process," *IEEE Trans. Electron Devices*, vol. 52, no. 10, pp. 2317–2322, Oct. 2005.

[20] A. Mohanbabu, N. Mohankumar, D. Godwin Raj, P. Sarkar, and S. K. Saha, "Efficient III-nitride MIS-HEMT devices with high-$K$ gate dielectric for high-power switching boost converter circuits," *Superlattices Microstruct.*, vol. 103, pp. 270–284, Mar. 2017.

[21] A. Mohanbabu, N. Anbuselvan, N. Mohankumar, D. Godwinraj, and C. K. Sarkar, "Modeling of sheet carrier density and microwave frequency characteristics in spacer based AlGaN/AlN/GaN HEMT devices," *Solid-State Electron.*, vol. 91, pp. 44–52, Jan. 2014.

[22] A. Mohanbabu, N. Mohankumar, D. Godwin Raj, P. Sarkar, and S. K. Saha, "Device characteristics of enhancement mode double heterostructure DH-HEMT with boron-doped GaN gate cap layer for full-bridge inverter circuit," *Int. J. Numer. Model., Electron. Netw., Devices Fields*, vol. 31, no. 3, p. e2276, Aug. 2017.

[23] Y. U. Tarauni, D. J. Thiruvadigal, B. Joseph, and A. Mohanbabu, "Optimization of enhancement mode P-type mg-doped In0.2Ga0.8N cap gate DH-HEMT for low-loss high power efficient boost converter circuits," *Mater. Sci. Semicond. Process.*, vol. 103, Nov. 2019, Art. no. 104624.

[24] B. Subramanian, M. Anandan, S. Veerappan, M. Panneerselvam, M. Wasim, S. K. Radhakrishnan, P. Pechimuthu, Y. K. Verma, S. N. Vivekanandhan, and E. Raju, "Switching transient analysis and characterization of an E-mode B-doped GaN-capped AlGaN DH-HEMT with a freewheeling Schottky barrier diode (SBD)," *J. Electron. Mater.*, vol. 49, no. 7, pp. 4091–4099, Jul. 2020.

[25] O. Ambacher, J. Smart, J. R. Shealy, N. G. Weimann, K. Chu, M. Murphy, W. J. Schaff, L. F. Eastman, R. Dimitrov, L. Wittmer, M. Stutzmann, W. Rieger, and J. Hilsenbeck, "Two-dimensional electron gases induced by spontaneous and piezoelectric polarization charges in N- and ga-face AlGaN/GaN heterostructures," *J. Appl. Phys.*, vol. 85, no. 6, pp. 3222–3233, Mar. 1999.

[26] S. Strauss, A. Erlebach, T. Cilento, D. Marcon, S. Stoffels, and B. Bakeroot, "TCAD methodology for simulation of GaN-HEMT power devices," in *Proc. IEEE 26th Int. Symp. Power Semiconductor Devices IC's (ISPSD)*, Jun. 2014, pp. 257–260.

[27] I. H. Oğuzman, E. Bellotti, K. F. Brennan, J. Kolník, R. Wang, and P. P. Ruden, "Theory of hole initiated impact ionization in bulk zincblende and wurtzite GaN," *J. Appl. Phys.*, vol. 81, no. 12, pp. 7827–7834, Jun. 1997.

[28] T. T. Mnatsakanov, M. E. Levinshtein, L. I. Pomortseva, S. N. Yurkov, G. S. Simin, and M. Asif Khan, "Carrier mobility model for GaN," *Solid-State Electron.*, vol. 47, no. 1, pp. 111–115, Jan. 2003.

[29] W. Mao, H. Wang, P. Shi, C. Yang, Y. Zhang, X. Zheng, C. Wang, J. Zhang, and Y. Hao, "Study of GaN-based step-doping superjunction CAVET for further improvement of breakdown voltage and specific on-resistance," *Semicond. Sci. Technol.*, vol. 33, no. 2, Jan. 2018, Art. no. 025005.

[30] W. Mao, H.-Y. Wang, P.-H. Shi, X.-F. Wang, M. Du, X.-F. Zheng, C. Wang, X.-H. Ma, J.-C. Zhang, and Y. Hao, "Low specific on-resistance GaN-based vertical heterostructure field effect transistors with nonuniform doping superjunctions," *Chin. Phys. B*, vol. 27, no. 4, Apr. 2018, Art. no. 047305.

[31] W. Mao, J. S. Fan, M. Du, J. F. Zhang, X. F. Zheng, C. Wang, and X. H. Ma, "Analysis of the modulation mechanisms of the electric field and breakdown performance in AlGaN/GaN HEMT with a T-shaped field-plate," *Chin. Phys. B*, vol. 25, no. 12, pp. 430–434, Dec. 2016.

[32] T. Paskova, D. A. Hanser, and K. R. Evans, "GaN substrates for III-nitride devices," *Proc. IEEE*, vol. 98, no. 7, pp. 1324–1338, Jul. 2010.

[33] H. Nie, Q. Diduck, B. Alvarez, A. P. Edwards, B. M. Kayes, M. Zhang, G. Ye, T. Prunty, D. Bour, and I. C. Kizilyalli, "1.5-kV and 2.2-m$\Omega$-cm$^2$ vertical GaN transistors on bulk-GaN substrates," *IEEE Electron Device Lett.*, vol. 35, no. 9, pp. 939–941, Sep. 2014.

[34] J. Tourret, O. Gourmala, Y. André, A. Trassoudaine, E. Gil, D. Castelluci, and R. Cadoret, "A complete crystallographic study of GaN epitaxial morphologies in selective area growth by hydride vapour phase epitaxy (SAG-HVPE)," *J. Cryst. Growth*, vol. 311, no. 6, pp. 1460–1465, Mar. 2009.

[35] C. Yang, H. Fu, V. N. Kumar, K. Fu, H. Liu, X. Huang, T.-H. Yang, H. Chen, J. Zhou, X. Deng, J. Montes, F. A. Ponce, D. Vasileska, and Y. Zhao, "GaN vertical-channel junction field-effect transistors with regrown p-GaN by MOCVD," *IEEE Trans. Electron Devices*, vol. 67, no. 10, pp. 3972–3977, Oct. 2020.

[36] K. Fu, H. Fu, X. Huang, H. Chen, T.-H. Yang, J. Montes, C. Yang, J. Zhou, and Y. Zhao, "Demonstration of 1.27 kV Etch-Then-Regrow GaN $p$ -$n$ junctions with low leakage for GaN power electronics," *IEEE Electron Device Lett.*, vol. 40, no. 11, pp. 1728–1731, Nov. 2019.

[37] P.-Y. Su, H. Liu, C. Yang, K. Fu, H. Fu, Y. Zhao, and F. A. Ponce, "Lateral and vertical growth of mg-doped GaN on trench-patterned GaN films," *Appl. Phys. Lett.*, vol. 117, no. 10, Sep. 2020, Art. no. 102110.

[38] H. Liu, H. Fu, K. Fu, S. R. Alugubelli, P.-Y. Su, Y. Zhao, and F. A. Ponce, "Non-uniform MG distribution in GaN epilayers grown on mesa structures for applications in GaN power electronics," *Appl. Phys. Lett.*, vol. 114, no. 8, Feb. 2019, Art. no. 082102.


**MIAO ZHANG** received the B.S. degree in electronic science and technology from Hohai University, China, in 2019. He is currently pursuing the M.S. degree in microelectronics and solid state electronics with South China Normal University, China.

**ZHIYOU GUO** was born in Liaoning, China, in 1959. Since 2006, he has been with South China Normal University, China, where he is currently a Professor. His research interests include wide band gap semiconductor materials and devices and GaN-based micro LED devices for visible light communication.

**YONG HUANG** received the B.S. degree from Foshan University, in 2004, the M.S. degree from the South China University of Technology, in 2007, and the Ph.D. degree from South China Normal University, in 2018. His research interests include GaN-based visible light communication LED and micro-LED.

**YUAN LI** received the B.S. degree in information display and photoelectric technology from the South China University of Technology, China, in 2016. He is currently pursuing the Ph.D. degree in electronics science and technology with South China Normal University, China.

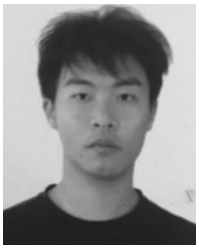

**JIANCHENG MA** received the B.S. degree in opto-electronics information science and engineering from the Hunan University of Science and Technology, China, in 2019. He is currently pursuing the M.S. degree in optical engineering with South China Normal University.

**XIAOYU XIA** received the B.S. degree in electronic science and technology from Hubei University, China, in 2018. She is currently pursuing the M.S. degree in microelectronics and solid state electronics with South China Normal University.

**XIUYANG TAN** received the B.S. degree from the University of Electronic Science and Technology of China, in 2018. She is currently pursuing the M.S. degree in optics with South China Normal University, China.

**FAN XIA** received the B.S. degree from the College of Physics and Electronic Information, Anhui Normal University, China, in 2019. She is currently pursuing the M.S. degree in microelectronics and solid state electronics with South China Normal University, Guangzhou.

**HUIQING SUN** was born in Liaoning, China, in 1963. Since 2004, she has been with South China Normal University, China, where she is currently an Associate Professor. Her research interest includes wide band gap semiconductor materials and devices.